Non-Hermitian Spatial Symmetries and Their Stabilized Normal and Exceptional Topological Semimetals

W. B. Rui,* Zhen Zheng, Chenjie Wang,† and Z. D. Wang‡
Department of Physics and HKU-UCAS Joint Institute for Theoretical and Computational Physics at Hong Kong, The University of Hong Kong, Pokfulam Road, Hong Kong, China

(Received 25 November 2021; revised 18 March 2022; accepted 4 May 2022; published 1 June 2022)

We study non-Hermitian spatial symmetries—a class of symmetries that have no counterparts in Hermitian systems—and study how normal and exceptional semimetals can be stabilized by these symmetries. Different from internal ones, spatial symmetries act nonlocally in momentum space and enforce global constraints on both band degeneracies and topological quantities at different locations. In deriving general constraints on band degeneracies and topological invariants, we demonstrate that non-Hermitian spatial symmetries are on an equal footing with, but are essentially different from Hermitian ones. First, we discover the nonlocal Hermitian conjugate pair of exceptional or normal band degeneracies that are enforced by non-Hermitian spatial symmetries. Remarkably, we find that these pairs lead to the symmetry-enforced violation of the Fermion doubling theorem in the long-time limit. Second, with the topological constraints, we unravel that a certain exceptional manifold is only compatible with and stabilized by non-Hermitian spatial symmetries but is intrinsically incompatible with Hermitian spatial symmetries. We illustrate these findings using two three-dimensional models of a non-Hermitian Weyl semimetal and an exceptional unconventional Weyl semimetal. Experimental cold-atom realizations of both models are also proposed.

DOI: 10.1103/PhysRevLett.128.226401

Introduction.—Symmetry serves as a guiding principle in the study of topological phases. A hallmark is the classification of topological phases with internal symmetries [1–3] or spatial symmetries (i.e., topological crystalline phases) [3–17]. Recently, the study has been extended into the non-Hermitian regime [18–28]. In non-Hermitian systems, besides normal semimetals with non-defective degeneracies, there are exceptional semimetals characterized by exceptional points (EPs) [29–32], at which the Hamiltonian is defective and the energy bands are also degenerate. These degeneracies may collectively form normal or exceptional manifolds [33], such as rings, surfaces, and complex structures like a nexus [34–46].

Internal symmetries, although widely studied in non-Hermitian systems [47–55], seem to be playing a small role in stabilizing the global configuration of the above-mentioned band degeneracies and their formed manifolds. Thus, it is then natural to resort to spatial symmetries. Like internal symmetries that are greatly ramified by non-Hermiticity [51–56], spatial symmetries also come in different classes, such as the Hermitian and non-Hermitian classes—see Eqs. (1) and (2) for definitions. So far, it is unclear whether and how different classes of spatial symmetries can stabilize band degeneracies and constrain topological properties in non-Hermitian systems.

In this Letter, we focus on non-Hermitian spatial symmetries and demonstrate how they characterize and stabilize normal and exceptional topological semimetals. First, we show that both normal and exceptional band degeneracies are preserved under symmetry operations, similar to Hermitian cases. But there is a stark difference: the symmetry-related band degeneracies form a nonlocal Hermitian conjugate pair in momentum space and, thus, must possess opposite imaginary energies. As imaginary energy determines the inverse lifetime, only half of these degeneracies survive in the long-time limit, leading to the violation of the Fermion doubling theorem, as shown in Fig. 1(b). Second, we show that compared to Hermitian ones, non-Hermitian spatial symmetries play an equivalent role but act differently in constraining the topological quantities, including Wilson loops, Chern numbers, and winding numbers. We explore the exceptional unconventional Weyl semimetal to show that certain exceptional manifolds [e.g., Fig. 3(b)] are compatible with and can only be stabilized by non-Hermitian spatial symmetries, but they are intrinsically incompatible with Hermitian spatial symmetries due to constraints on topological quantities. We also discuss possible realizations of our models in cold-atomic systems.

Non-Hermitian spatial symmetries.—Consider a crystal or lattice system with lattice-translation symmetries, so that the Hamiltonian can be transformed into momentum space. If the system respects a crystalline symmetry, the Hamiltonian usually transforms as

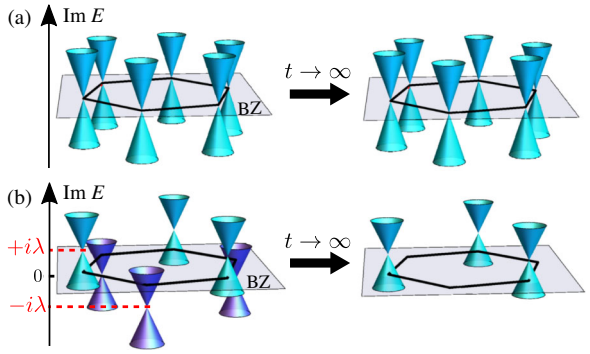

FIG. 1. Schematic for the violation of the Fermion doubling theorem enforced by the non-Hermitian spatial symmetry in the long-time limit (b). For the Hermitian spatial symmetry in (a), the theorem is still respected. Here, the six-fold rotation symmetry is taken for illustration.

$$\mathcal{G}\mathcal{H}(\mathbf{k})\mathcal{G}^{-1} = \mathcal{H}(g\mathbf{k}), \tag{1}$$

where we take $\mathcal{G}$ to be unitary and g transforms the crystal momentum $\mathbf{k}$. In Hermitian systems, the above transformation is equivalent to

$$\mathcal{G}\mathcal{H}(\mathbf{k})\mathcal{G}^{-1} = \mathcal{H}^{\dagger}(g\mathbf{k}). \tag{2}$$

However, the equivalence no longer holds in non-Hermitian systems as $\mathcal{H}^{\dagger}(\mathbf{k}) \neq \mathcal{H}(\mathbf{k})$. Accordingly, Eqs. (1) and (2) describe different classes of symmetries. Such a ramification by non-Hermiticity is similar to that of nonspatial symmetries. The latter has been systematically studied, e.g., in Ref. [52], which shows that there are 38-fold symmetry classes, far beyond the celebrated Altland-Zirnbauer tenfold classes in Hermitian systems. We will refer to those satisfying (1) as "Hermitian spatial symmetries" and those satisfying (2) as "non-Hermitian spatial symmetries." Note that $\mathcal{G}$ can also be antiunitary. However, we focus on the unitary case below.

Let $|\Psi_{L,n}(\mathbf{k})\rangle$ and $|\Psi_{R,n}(\mathbf{k})\rangle$ be the left and right eigenvectors of the non-Hermitian Hamiltonian $\mathcal{H}(\mathbf{k})$, respectively, where n is the band index. The two vectors satisfy $\mathcal{H}(\mathbf{k})|\Psi_{R,n}(\mathbf{k})\rangle = E_n(\mathbf{k})|\Psi_{R,n}(\mathbf{k})\rangle$ and $\mathcal{H}^{\dagger}(\mathbf{k})|\Psi_{L,n}(\mathbf{k})\rangle = E_n^*(\mathbf{k})|\Psi_{L,n}(\mathbf{k})\rangle$. They are different in general and form a biorthonormal basis, satisfying $\langle\Psi_{L,m}(\mathbf{k})|\Psi_{R,n}(\mathbf{k})\rangle = \delta_{mn}$. If $\mathcal{H}(\mathbf{k})$ admits a non-Hermitian spatial symmetry $\mathcal{G}$ satisfying Eq. (2), one can show that

$$\begin{aligned}\mathcal{H}^{\dagger}(g\mathbf{k})\mathcal{G}|\Psi_{R,n}(\mathbf{k})\rangle &= E_n(\mathbf{k})\mathcal{G}|\Psi_{R,n}(\mathbf{k})\rangle,\\ \mathcal{H}(g\mathbf{k})\mathcal{G}|\Psi_{L,n}(\mathbf{k})\rangle &= E_n^*(\mathbf{k})\mathcal{G}|\Psi_{L,n}(\mathbf{k})\rangle.\end{aligned} \tag{3}$$

Accordingly, every right (left) eigensystem $\{|\Psi_{R,n}(\mathbf{k})\rangle, E_n(\mathbf{k})\}$ ($\{|\Psi_{L,n}(\mathbf{k})\rangle, E_n^*(\mathbf{k})\}$) at $\mathbf{k}$ is mapped to a left (right) eigensystem $\{\mathcal{G}|\Psi_{R,n}(\mathbf{k})\rangle, E_n^*(\mathbf{k})\}$ ($\{\mathcal{G}|\Psi_{L,n}(\mathbf{k})\rangle, E_n(\mathbf{k})\}$) at $g\mathbf{k}$. As $\mathcal{G}$ is invertible, this map is a one-to-one correspondence. On the other hand, a Hermitian symmetry $\mathcal{G}$ maps a right (left) eigensystem to a right (left) eigensystem.

Nonlocal Hermitian conjugate pair of normal or exceptional degeneracies.—The non-Hermitian symmetry $\mathcal{G}$ also maps between band degeneracies nonlocally, but in a way different from a Hermitian one. Consider a degeneracy at momentum $\mathbf{k}_D$. The Hamiltonian $\mathcal{H}(\mathbf{k}_D)$ can be transformed by an invertible matrix $\mathcal{P}$ as

$$\mathcal{P}^{-1}\mathcal{H}(\mathbf{k}_D)\mathcal{P} = \mathcal{J}(\mathbf{k}_D), \quad \mathcal{J}(\mathbf{k}_D) = E(\mathbf{k}_D)\mathbb{1} + \sigma\mathcal{N}. \tag{4}$$

Here, $\mathbb{1}$ is the identity matrix and $\mathcal{N}$ the nilpotent matrix defined by $\mathcal{N}_{ij} = \delta_{i,j-1}$. $\sigma = 0$ corresponds to normal degeneracies, and $\sigma = 1$ corresponds to a Jordan block for exceptional degeneracies, i.e., EPs. In the presence of a non-Hermitian symmetry (2), it can be derived that

$$\tilde{\mathcal{P}}\mathcal{H}(g\mathbf{k}_D)\tilde{\mathcal{P}}^{-1} = \mathcal{J}^{\dagger}(\mathbf{k}_D), \tag{5}$$

where $\tilde{\mathcal{P}} = \mathcal{P}^{\dagger}\mathcal{G}^{\dagger}$ is invertible. By comparing Eqs. (4) and (5), we can see that $\mathcal{H}(g\mathbf{k}_D)$ is brought to the same $\mathcal{J}(\mathbf{k}_D)$ as $\mathcal{H}(\mathbf{k}_D)$, meaning that the normal or exceptional degeneracy is preserved under the symmetry operation. However, a stark difference is the Hermitian conjugation in (5), which does not appear for the Hermitian spatial symmetry. It makes the symmetry-related degeneracies form nonlocal Hermitian conjugate pairs in momentum space.

Symmetry-enforced violation of Fermion doubling theorem in the long-time limit.—For topological point degeneracies, such as Weyl points, they must come in pairs on lattice according to the Fermion doubling theorem [57–59]. Recently, this concept has been extended to include EPs in non-Hermitian systems [60]. Under non-Hermitian spatial symmetry, as the two symmetry-related normal or exceptional band degeneracies form a nonlocal Hermitian conjugate pair, their energies obey

$$E(g\mathbf{k}_D) = E^*(\mathbf{k}_D). \tag{6}$$

It means that the two degeneracies are distinguishable by their opposite imaginary energies, as shown by the blue and cyan cones in the left panel of Fig. 1(b). Such a distinction is not possible under Hermitian spatial symmetry with $E(g\mathbf{k}_D) = E(\mathbf{k}_D)$, as shown in Fig. 1(a).

Remarkably, the above symmetry-enforced separation of imaginary energy between degeneracies leads to anomalous behaviors. In the long-time limit [55,61], as the imaginary energy determines the inverse lifetime, only the modes at the degeneracies with positive imaginary energies survive. Thus, effectively, only half of the symmetry-related degeneracies (normal or exceptional) exist, leading to the violation of the Fermion doubling theorem in the long-time limit, as shown in Fig. 1(b). Note that this cannot happen for a Hermitian symmetry $\mathcal{G}$.

Topological quantities: Wilson loop, Chern number, and winding number.—The non-Hermitian spatial symmetries play an equivalent role but act in a different way than Hermitian spatial symmetries in constraining topological quantities [62–65]. For biorthonormal eigenstates, Wilson loops in non-Hermitian systems can be defined as [66,67]

$$\mathcal{W}_{\mathcal{L}}^{\alpha\bar{\alpha}} = \overline{\exp}\left[-\oint_{\mathbf{k}_0} d\mathbf{k}\mathcal{A}^{\alpha\bar{\alpha}}(\mathbf{k})\right], \tag{7}$$

where $\alpha = R$, L (with $\bar{R} = L$ and $\bar{L} = R$), $\mathcal{L}$ is a loop in momentum space with $\mathbf{k}_0$ being a base point, and "$\overline{\exp}$" denotes that the integral is path ordered. The non-Abelian Berry connection is defined as $\mathcal{A}_{mn}^{\alpha\bar{\alpha}}(\mathbf{k}) = \langle\Psi_{\alpha,m}(\mathbf{k})|\partial_{\mathbf{k}}|\Psi_{\bar{\alpha},n}(\mathbf{k})\rangle$ for a set of bands that are separated from other bands along the loop $\mathcal{L}$. The Wilson loop $\mathcal{W}_{\mathcal{L}}^{\alpha\bar{\alpha}}$ is invariant under a basis transformation (gauge transformation) only in the Abelian case (i.e., a single band). For multiple bands, one needs to consider the determinant

$$\det(\mathcal{W}_{\mathcal{L}}^{\alpha\bar{\alpha}}) = \exp\left(a_{\mathcal{L}}^{\alpha\bar{\alpha}} + i\gamma_{\mathcal{L}}^{\alpha\bar{\alpha}}\right), \tag{8}$$

where both $a_{\mathcal{L}}^{\alpha\bar{\alpha}}$ and $\gamma_{\mathcal{L}}^{\alpha\bar{\alpha}}$ are real. The phase $\gamma_{\mathcal{L}}^{\alpha\bar{\alpha}}$ is the Berry phase. We show in the Supplemental Material (SM) [68] that $a_{\mathcal{L}}^{LR} = -a_{\mathcal{L}}^{RL}$, $\gamma_{\mathcal{L}}^{LR} = \gamma_{\mathcal{L}}^{RL}$.

With a non-Hermitian spatial symmetry in (2), the Wilson loop satisfies the following relation (see SM [68] for details):

$$\mathcal{W}_{\mathcal{L}}^{\alpha\bar{\alpha}} = \mathcal{S}_{g,\alpha}^{\dagger}(\mathbf{k}_0)\tilde{\mathcal{W}}_{g\mathcal{L}}^{\bar{\alpha}\alpha}\mathcal{S}_{g,\bar{\alpha}}(\mathbf{k}_0), \tag{9}$$

where $g\mathcal{L}$ is the image of $\mathcal{L}$ under $\mathcal{G}$, and the sewing matrix $\mathcal{S}_{g,\alpha}^{\tilde{n}n}(\mathbf{k}) = \langle\Psi_{\alpha,\tilde{n}}(g\mathbf{k})|\mathcal{G}|\Psi_{\alpha,n}(\mathbf{k})\rangle$. Here, "$\tilde{n}$" indexes the bands associated with the states $\mathcal{G}|\Psi_{\alpha,n}(\mathbf{k})\rangle$, which are not necessarily the same as those of $|\Psi_{\alpha,n}(\mathbf{k})\rangle$, and $\tilde{\mathcal{W}}_{g\mathcal{L}}^{\alpha\bar{\alpha}}$ is the corresponding Wilson loop. Unitarity of $\mathcal{G}$ leads to $\mathcal{S}_{g,\alpha}^{\dagger}(\mathbf{k})\mathcal{S}_{g,\bar{\alpha}}(\mathbf{k}) = \mathbb{1}$. Taking the determinant on both sides of (9), we obtain $\tilde{a}_{g\mathcal{L}}^{\alpha\bar{\alpha}} = a_{\mathcal{L}}^{\bar{\alpha}\alpha}$, $\tilde{\gamma}_{g\mathcal{L}}^{\alpha\bar{\alpha}} = \gamma_{\mathcal{L}}^{\bar{\alpha}\alpha}$. Instead, if $\mathcal{G}$ is a Hermitian symmetry, we have $\tilde{a}_{g\mathcal{L}}^{\alpha\bar{\alpha}} = a_{\mathcal{L}}^{\alpha\bar{\alpha}}$ and $\tilde{\gamma}_{g\mathcal{L}}^{\alpha\bar{\alpha}} = \gamma_{\mathcal{L}}^{\alpha\bar{\alpha}}$.

Chern numbers can also be defined in non-Hermitian systems. The non-Abelian Berry curvature is defined as $\mathcal{B}^{\alpha\bar{\alpha}} = i\nabla\times\mathcal{A}^{\alpha\bar{\alpha}} + i\mathcal{A}^{\alpha\bar{\alpha}}\times\mathcal{A}^{\alpha\bar{\alpha}}$. Then, associated with every closed surface Σ on which a set of energy bands are separate from others, the Chern number is given by

$$C_{\Sigma} = \frac{1}{2\pi}\mathrm{Re}\int_{\Sigma} d\mathbf{S}\cdot\mathrm{tr}(\mathcal{B}^{\alpha\bar{\alpha}}). \tag{10}$$

We show, in the SM [68], that C_{Σ} is independent of α and that it takes integer values. Similar to the Berry phase, one can show that $C_{\Sigma} = \tilde{C}_{g\Sigma}$, where $g\Sigma$ is the image of Σ under $\mathcal{G}$, and $\tilde{C}_{g\Sigma}$ is associated with the bands of $\mathcal{G}|\Psi_{R,n}(\mathbf{k})\rangle$.

Now, we turn to the topology of EPs. As proved in the SM [68], for order-2 EPs in three-dimensional (3D) systems, they generally form exceptional lines (ELs). Assuming a gap around such an EL, a winding number can be defined [22,47]

$$W(\mathbf{k}_{\mathrm{EP}}) = \frac{1}{2\pi i}\oint_{S^1} d\mathbf{k}\cdot\nabla_{\mathbf{k}}\log\det[\mathcal{H}(\mathbf{k}) - E(\mathbf{k}_{\mathrm{EP}})], \tag{11}$$

where S^1 is a loop that encircles the EL and $\mathbf{k}_{\mathrm{EP}}$ is any point on the EL. The integral (11) needs an orientation on S^1 to be unambiguous. It can be done by assigning an orientation to the EL first, which then induces an orientation on S^1 through the right-hand rule. Changing the orientation of the EL gives a minus sign to $W(\mathbf{k}_{\mathrm{EP}})$.

In the presence of spatial symmetry $\mathcal{G}$, we show in the SM [68] that

$$W(g\mathbf{k}_{\mathrm{EP}}) = \zeta\sigma(\mathbf{k}_{\mathrm{EP}})\sigma(g)W(\mathbf{k}_{\mathrm{EP}}), \tag{12}$$

where $\zeta = +1$ if $\mathcal{G}$ is a Hermitian symmetry, and $\zeta = -1$ if $\mathcal{G}$ is a non-Hermitian symmetry. The factor $\sigma(\mathbf{k}_{\mathrm{EP}}) = \sigma(g\mathbf{k}_{\mathrm{EP}}, \mathbf{k}_{\mathrm{EP}}) = 1$ if the orientations of the ELs at $\mathbf{k}_{\mathrm{EP}}$ and $g\mathbf{k}_{\mathrm{EP}}$ match under $\mathcal{G}$, and $\sigma(g\mathbf{k}_{\mathrm{EP}}, \mathbf{k}_{\mathrm{EP}}) = -1$, otherwise. The factor $\sigma(g) = 1$ or -1, if $\mathcal{G}$ preserves (e.g., rotation) or reverses (e.g., mirror reflection) the chirality of the momentum space, respectively.

Non-Hermitian Weyl semimetals.—With the above general results, we proceed to discuss two concrete models. The first model is a normal Weyl semimetal protected by a non-Hermitian inversion symmetry. In the long-time limit, there is only one Weyl point in effect, violating the Fermion doubling theorem. The cold-atom realization of this model can be found in the SM [68]. The model Hamiltonian in momentum space reads

$$\begin{aligned}\mathcal{H}(\mathbf{k}) = {} & A\sin k_x\tau_1\sigma_1 + A\sin k_y\tau_1\sigma_2 + A\sin k_z\tau_1\sigma_3 \\ & + M(\mathbf{k})\tau_3\sigma_0 + k_0\tau_0\sigma_3 + i\lambda\tau_1\sigma_0,\end{aligned} \tag{13}$$

where $M(\mathbf{k}) = (t\cos k_x + t\cos k_y + t\cos k_z - M)$ and M, A, t, k_0, λ are real parameters. The system respects the non-Hermitian inversion symmetry $\mathcal{I} = \tau_3\sigma_0$ as

$$\mathcal{I}\mathcal{H}(\mathbf{k})\mathcal{I}^{-1} = \mathcal{H}(-\mathbf{k})^{\dagger}. \tag{14}$$

TABLE I. Transformation rules of different topological quantities under Hermitian and non-Hermitian spatial symmetries. We have denoted $\tilde{W} \equiv W(g\mathbf{k}_{\mathrm{EP}})$ and $W \equiv W(\mathbf{k}_{\mathrm{EP}})$, see Eq. (12). Here, no. is short for number.

	Hermitian	Non-Hermitian
Wilson loop	$\tilde{a}_{g\mathcal{L}}^{\alpha\bar{\alpha}} = a_{\mathcal{L}}^{\alpha\bar{\alpha}}$ $\tilde{\gamma}_{g\mathcal{L}}^{\alpha\bar{\alpha}} = \gamma_{\mathcal{L}}^{\alpha\bar{\alpha}}$	$\tilde{a}_{g\mathcal{L}}^{\alpha\bar{\alpha}} = a_{\mathcal{L}}^{\bar{\alpha}\alpha}$ $\tilde{\gamma}_{g\mathcal{L}}^{\alpha\bar{\alpha}} = \gamma_{\mathcal{L}}^{\bar{\alpha}\alpha}$
Chern no.	$\tilde{C}_{g\Sigma} = C_{\Sigma}$	$\tilde{C}_{g\Sigma} = C_{\Sigma}$
Winding no.	$\tilde{W} = +\sigma(\mathbf{k}_{\mathrm{EP}})\sigma(g)W$	$\tilde{W} = -\sigma(\mathbf{k}_{\mathrm{EP}})\sigma(g)W$

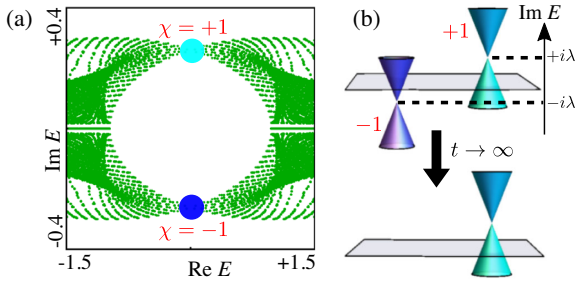

FIG. 2. (a) The energy spectrum for the Weyl semimetal protected by the non-Hermitian inversion symmetry. (b) The two Weyl points possess opposite imaginary energies due to the symmetry, which leads to a single Weyl point on lattice in the long-time limit. The parameters in the model (13) are $A = t = k_0 = 1.0$, $M = 3.0$, and $\lambda = 0.3$.

As shown in Fig. 2, for the chosen parameters, this model features two Weyl points (WPs) whose low-energy effective models can be obtained as

$$h_{\mathrm{WP1}}(\delta\mathbf{k}) = +\delta\mathbf{k}\cdot\boldsymbol{\sigma} + i\lambda\sigma_0, \qquad \mathbf{k} = (0,0,-k_0);$$
$$h_{\mathrm{WP2}}(\delta\mathbf{k}) = -\delta\mathbf{k}\cdot\boldsymbol{\sigma} - i\lambda\sigma_0, \qquad \mathbf{k} = (0,0,+k_0). \tag{15}$$

As the two Weyl points with opposite chiralities ($\chi = \pm 1$) are connected by the non-Hermitian symmetry, they form a nonlocal Hermitian conjugate pair of normal degeneracies and possess opposite imaginary energies of $\pm i\lambda$.

We use the time-evolution operator $\mathcal{U}(\mathbf{k},t) = \mathcal{T}\exp\left[-i/\hbar\int_0^t \mathcal{H}(\mathbf{k})dt'\right]$ ($\mathcal{T}$: time ordering), which is generally not unitary in non-Hermitian systems [76], to investigate the dynamics. After a sufficiently long time, i.e., $t \gg \hbar/\lambda$, the Weyl point described by $h_{\mathrm{WP2}}(\delta\mathbf{k})$ with $-i\lambda$ vanishes due to the exponentially decaying factor in its time-evolution operator. Thus, in the long-time limit, only the Weyl point described by $h_{\mathrm{WP1}}(\delta\mathbf{k})$ with imaginary energy $+i\lambda$ survives, leading to the violation of the Fermion doubling theorem, as shown in Fig. 2(b).

Exceptional unconventional Weyl semimetals.—Next, we study a non-Hermitian extension of unconventional Weyl semimetals, where the momentum space hosts monopoles of charge ± 2. This model demonstrates how non-Hermitian spatial symmetries can stabilize exceptional manifolds in a different way from the Hermitian ones and illustrate the transformation rules of topological quantities in Table I. We discuss a cold-atom realization of this model in the SM [68].

The momentum-space Hamiltonian of our model reads

$$\begin{aligned}\mathcal{H}^w(\mathbf{k}) &= \mathcal{H}_0^w(\mathbf{k}) + \mathcal{H}_1^w(\mathbf{k}),\\ \mathcal{H}_0^w(\mathbf{k}) &= 2A(\cos k_x - \cos k_y)\sigma_1 + 2A\sin k_x \sin k_y \sigma_2\\ &\quad + [M_0 - 2t_\parallel(\cos k_x + \cos k_y) - 2t_z\cos k_z]\sigma_3,\\ \mathcal{H}_1^w(\mathbf{k}) &= i\lambda\sigma_1,\end{aligned} \tag{16}$$

where all parameters M_0, $t_\parallel$, t_z, A, and λ are real. The unperturbed Hamiltonian $\mathcal{H}_0^w$ respects a normal fourfold rotation symmetry $\mathcal{C}_{4z} = \sigma_3$, $\mathcal{C}_{4z}\mathcal{H}_0^w(\mathbf{k})\mathcal{C}_{4z}^{-1} = \mathcal{H}_0^w(R_{4z}\mathbf{k})$ with $R_{4z}(k_x,k_y,k_z) = (k_y,-k_x,k_z)$. It has two Weyl points with monopole charge ± 2, located at $\mathbf{K}_\pm = [0,0,\pm\arccos(M_0 - 4t_\parallel)/2t_z]$, which are stabilized by the Hermitian $\mathcal{C}_{4z}$ symmetry [77]. With the non-Hermitian $\mathcal{H}_1^w$ included, the Hermitian symmetry is broken as $[\mathcal{C}_{4z}, i\lambda\sigma_1] \neq 0$. However, as a non-Hermitain symmetry, $\mathcal{C}_{4z}$ is still preserved, which reads

$$\mathcal{C}_{4z}\mathcal{H}^w(k_x,k_y,k_z)\mathcal{C}_{4z}^{-1} = \mathcal{H}^w(k_y,-k_x,k_z)^\dagger. \tag{17}$$

Figure 3(a) shows the exceptional manifold of the model, and Fig. 3(b) shows an enlargement around $\mathbf{K}_+$. Each of the original Weyl points turns into four rotation-symmetric ELs that jointly terminate on the rotation axis. All EPs including those on the axis are of order 2, with a winding number of $W(\mathbf{k}_{\mathrm{EP}}) = \pm 1$. As shown by the right panel of Fig. 3(b), the energy spectrum and EPs in the 2D k_xk_y

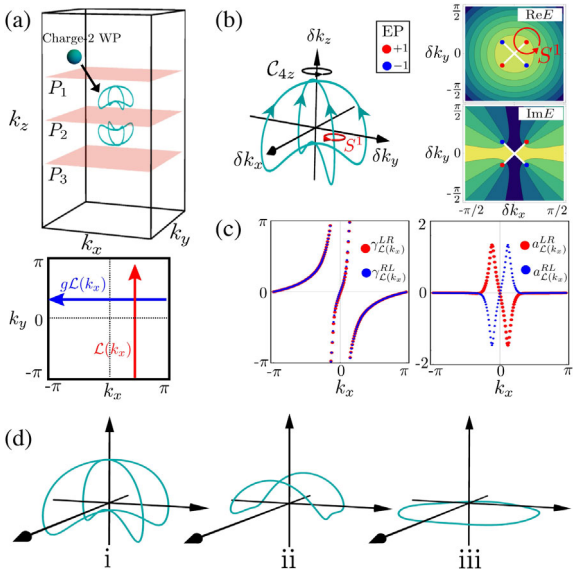

FIG. 3. (a) The non-Hermitian spatial symmetry preserving term turns an unconventional Weyl point into exceptional lines (cyan lines). The lower panel shows the paths (red and blue arrows) for calculating the Wilson loop for $\mathcal{L}(k_x)$ and symmetry-related $g\mathcal{L}(k_x)$ on the P_2 plane. (b) Left: Zoom-in of the exceptional manifold (cyan) around $\mathbf{K}_+$. Right: Contour plots of the real (upper) and imaginary (lower) eigenenergies on the k_xk_y plane at $\delta k_z = 0$. Here, blue and red points are EPs with $W(\mathbf{k}_{\mathrm{EP}}) = +1$ and -1, respectively. (c) The Berry phase $\gamma_{\mathcal{L}}^{\alpha\bar{\alpha}}$ and the real exponent $a_{\mathcal{L}}^{\alpha\bar{\alpha}}$ for a family of noncontractible loops $\mathcal{L}:(k_x,-\pi,0)\to(k_x,\pi,0)$ with $k_x \in [-\pi,\pi]$ on the P_2 plane in (a), i.e., the red arrow. (d) Evolution of the exceptional manifold (cyan) for $\mathcal{H}^{w'}(\mathbf{k})$ in (18) with $\eta \in [0,1]$. The rotation $\mathcal{C}_{4z}$ is a non-Hermitian symmetry at $\eta = 0$ (i), a Hermitian symmetry at $\eta = 1$ (iii), and broken when $0 < \eta < 1$ (ii). The parameters in the model (16) are $A = t_z = t_\parallel = 1.0$, $M_0 = 5.5$, and $\lambda = 0.3$.

Brillouin zone (BZ) across $\mathbf{K}_+$ clearly exhibit a fourfold rotation symmetry. The relations below (8) are explicitly verified for a family of loops in Fig. 3(c). The transformation rules of Wilson loops under non-Hermitian spatial symmetry in Table I are also verified for the two loops related by $\mathcal{C}_{4z}$ symmetry [red and blue arrows in Fig. 3(a), lower panel], which can be found in the SM [68]. We further compute the Chern numbers on planes $\Sigma = P_1$, P_2, and P_3, shown by pink planes in Fig. 3(a), which are $C_{P_1} = 0$, $C_{P_2} = -2$, and $C_{P_3} = 0$, respectively. It implies that, between P_1 and P_2 and between P_2 and P_3, there must exist regions that are energetically degenerate, whose stability is guaranteed by the Chern number.

In fact, stability of the structure of this exceptional manifold—specifically, existence of the intersection points on the rotation axis—can be argued further at a topological level. Let us consider a modified Hamiltonian

$$\mathcal{H}^{w'}(\mathbf{k}) = \mathcal{H}_0^{w}(\mathbf{k}) + i\lambda[(1-\eta)\sigma_1 + \eta\sigma_3]. \tag{18}$$

When $\eta = 0$, $\mathcal{H}^{w'}$ reduces to $\mathcal{H}^{w}$. When $\eta = 1$, the non-Hermitian perturbation $i\lambda\sigma_3$ respects $\mathcal{C}_{4z}$ as a Hermitian symmetry. Accordingly, by tuning $\eta \in [0, 1]$, we achieve a transition from a non-Hermitian $\mathcal{C}_{4z}$ to a Hermitian $\mathcal{C}_{4z}$. When $0 < \eta < 1$, $\mathcal{C}_{4z}$ is not respected either as Hermitian or non-Hermitian symmetry.

Figure 3(d) shows the evolution of the exceptional manifold as η varies. It exhibits a fourfold rotation symmetry both at $\eta = 0$ and $\eta = 1$. The key difference is that there are exceptional intersection points on the rotation axis at $\eta = 0$, while the whole axis is nondegenerate at $\eta = 1$. This difference can be explained by the constraint (12). In order for ELs to terminate on the rotation axis, the total winding number must vanish such that

$$\sum_{n=0}^{3} W(g^n \mathbf{k}_{\mathrm{EP}}) = 0. \tag{19}$$

If $\mathcal{C}_{4z}$ is Hermitian, Eqs. (12) and (19) together lead to $W(\mathbf{k}_{\mathrm{EP}}) = 0$. In other words, the exceptional manifold in Fig. 3[d(i)] is intrinsically incompatible with Hermitian symmetries. On the other hand, Eq. (19) is always satisfied for a non-Hermitian $\mathcal{C}_{4z}$ due to Eq. (12). Moreover, the exceptional intersection points are, indeed, protected by the non-Hermitian $\mathcal{C}_{4z}$ [68]. Thus, we conclude that non-Hermitian and Hermitian spatial symmetries may stabilize exceptional manifolds in very different manners.

Discussions.—Topological semimetals stabilized by non-Hermitian spatial symmetries provide a novel platform for investigating anomalous behaviors of unpaired normal or exceptional point degeneracies. An unpaired point degeneracy, such as a single Dirac point on the 3D topological insulator surface, represents an anomaly that may have unusual physical consequences [78–80]. We have demonstrated a mechanism for dynamically achieving unpaired point degeneracies, distinct from previous approaches using topological surface states [78,81]. This mechanism could be readily employed, e.g., in photonic experiments where EPs have been realized [18].

Finally, we remark that the two Weyl models are realizable not only in cold atoms, but also in other platforms like electrical circuits and photonics. We choose cold atoms for two reasons. First, cold atoms have the advantage for investigating both noninteracting and interacting systems and, thus, can extend our theory to many-particle physics [82,83]. The influence of the atomic many-body interaction can be manipulated further by Feshbach resonances [84,85]. Second, in cold atoms, there exist mature techniques for studying time-evolution dynamics [69,86–88] which is promising for realizing our theory about dynamically achieving unpaired degeneracies.

W. B. R. is grateful to Moritz M. Hirschmann for valuable discussions. This work was supported by the Key-Area Research and Development Program of GuangDong Province (Grant No. 2019B030330001), the CRF (Grants No. C6005-17G and No. C6009-20G) and GRF (Grant No. 17300220) of Hong Kong, and the NSFC/RGC JRS Grant No. N_HKU774/21. The authors also acknowledge support from Guangdong-Hong Kong Joint Laboratory of Quantum Matter.

*wbrui@hku.hk
†cjwang@hku.hk
‡zwang@hku.hk

[1] A. P. Schnyder, S. Ryu, A. Furusaki, and A. W. W. Ludwig, Phys. Rev. B **78**, 195125 (2008).
[2] A. Kitaev, AIP Conf. Proc. **1134**, 22 (2009).
[3] C.-K. Chiu, J. C. Y. Teo, A. P. Schnyder, and S. Ryu, Rev. Mod. Phys. **88**, 035005 (2016).
[4] L. Fu, Phys. Rev. Lett. **106**, 106802 (2011).
[5] Y. Tanaka, Z. Ren, T. Sato, K. Nakayama, S. Souma, T. Takahashi, K. Segawa, and Y. Ando, Nat. Phys. **8**, 800 (2012).
[6] P. Dziawa, B. J. Kowalski, K. Dybko, R. Buczko, A. Szczerbakow, M. Szot, E. Łusakowska, T. Balasubramanian, B. M. Wojek, M. H. Berntsen, O. Tjernberg, and T. Story, Nat. Mater. **11**, 1023 (2012).
[7] Y. Ando and L. Fu, Annu. Rev. Condens. Matter Phys. **6**, 361 (2015).
[8] C. Fang and L. Fu, Phys. Rev. B **91**, 161105(R) (2015).
[9] E. Khalaf, H. C. Po, A. Vishwanath, and H. Watanabe, Phys. Rev. X **8**, 031070 (2018).
[10] H. C. Po, A. Vishwanath, and H. Watanabe, Nat. Commun. **8**, 50 (2017).
[11] F. Tang, H. C. Po, A. Vishwanath, and X. Wan, Nature (London) **566**, 486 (2019).
[12] T. Zhang, Y. Jiang, Z. Song, H. Huang, Y. He, Z. Fang, H. Weng, and C. Fang, Nature (London) **566**, 475 (2019).
[13] M. G. Vergniory, L. Elcoro, C. Felser, N. Regnault, B. A. Bernevig, and Z. Wang, Nature (London) **566**, 480 (2019).

[14] J. Kruthoff, J. de Boer, J. van Wezel, C. L. Kane, and R.-J. Slager, Phys. Rev. X **7**, 041069 (2017).
[15] W. A. Benalcazar, B. A. Bernevig, and T. L. Hughes, Science **357**, 61 (2017).
[16] W. B. Rui, S.-B. Zhang, M. M. Hirschmann, Z. Zheng, A. P. Schnyder, B. Trauzettel, and Z. D. Wang, Phys. Rev. B **103**, 184510 (2021).
[17] W. B. Rui, Z. Zheng, M. M. Hirschmann, S.-B. Zhang, C. Wang, and Z. D. Wang, npj Quantum Mater. **7**, 15 (2022).
[18] H. Zhou, C. Peng, Y. Yoon, C. W. Hsu, K. A. Nelson, L. Fu, J. D. Joannopoulos, M. Soljacic, and B. Zhen, Science **359**, 1009 (2018).
[19] M. A. Bandres, S. Wittek, G. Harari, M. Parto, J. Ren, M. Segev, D. N. Christodoulides, and M. Khajavikhan, Science **359**, eaar4005 (2018).
[20] H. Zhao, X. Qiao, T. Wu, B. Midya, S. Longhi, and L. Feng, Science **365**, 1163 (2019).
[21] D. Leykam, K. Y. Bliokh, C. Huang, Y. D. Chong, and F. Nori, Phys. Rev. Lett. **118**, 040401 (2017).
[22] H. Shen, B. Zhen, and L. Fu, Phys. Rev. Lett. **120**, 146402 (2018).
[23] Z. Yang, A. P. Schnyder, J. Hu, and C.-K. Chiu, Phys. Rev. Lett. **126**, 086401 (2021).
[24] L. Xiao, T. Deng, K. Wang, G. Zhu, Z. Wang, W. Yi, and P. Xue, Nat. Phys. **16**, 761 (2020).
[25] R. Okugawa, R. Takahashi, and K. Yokomizo, Phys. Rev. B **103**, 205205 (2021).
[26] P. M. Vecsei, M. M. Denner, T. Neupert, and F. Schindler, Phys. Rev. B **103**, L201114 (2021).
[27] K. Shiozaki and S. Ono, Phys. Rev. B **104**, 035424 (2021).
[28] W. B. Rui, Y. X. Zhao, and A. P. Schnyder, Phys. Rev. B **99**, 241110(R) (2019).
[29] T. Kato, *Perturbation Theory for Linear Operators*, 2nd ed., Classics in Mathematics (Springer-Verlag, Berlin, 1995).
[30] V. V. Konotop, J. Yang, and D. A. Zezyulin, Rev. Mod. Phys. **88**, 035002 (2016).
[31] M.-A. Miri and A. Alù, Science **363**, eaar7709 (2019).
[32] C. H. Lee, Phys. Rev. Lett. **128**, 010402 (2022).
[33] Here, we abuse the term, "manifold." A normal or exceptional manifold may not be a manifold in the mathematical sense.
[34] Y. Xu, S.-T. Wang, and L.-M. Duan, Phys. Rev. Lett. **118**, 045701 (2017).
[35] T. Yoshida, R. Peters, N. Kawakami, and Y. Hatsugai, Phys. Rev. B **99**, 121101(R) (2019).
[36] A. Cerjan, S. Huang, M. Wang, K. P. Chen, Y. Chong, and M. C. Rechtsman, Nat. Photonics **13**, 623 (2019).
[37] Sayed Ali Akbar Ghorashi, T. Li, M. Sato, and T. L. Hughes, Phys. Rev. B **104**, L161116 (2021).
[38] T. Liu, J. J. He, Z. Yang, and F. Nori, Phys. Rev. Lett. **127**, 196801 (2021).
[39] W. B. Rui, M. M. Hirschmann, and A. P. Schnyder, Phys. Rev. B **100**, 245116 (2019).
[40] X. Zhang, K. Ding, X. Zhou, J. Xu, and D. Jin, Phys. Rev. Lett. **123**, 237202 (2019).
[41] H. Zhou, J. Y. Lee, S. Liu, and B. Zhen, Optica **6**, 190 (2019).
[42] X. Zhang, G. Li, Y. Liu, T. Tai, R. Thomale, and C. H. Lee, Commun. Phys. **4**, 47 (2021).
[43] W. Tang, X. Jiang, K. Ding, Y.-X. Xiao, Z.-Q. Zhang, C. T. Chan, and G. Ma, Science **370**, 1077 (2020).
[44] K. Wang, L. Xiao, J. C. Budich, W. Yi, and P. Xue, Phys. Rev. Lett. **127**, 026404 (2021).
[45] J. Carlström and E. J. Bergholtz, Phys. Rev. A **98**, 042114 (2018).
[46] P. He, J.-H. Fu, D.-W. Zhang, and S.-L. Zhu, Phys. Rev. A **102**, 023308 (2020).
[47] K. Kawabata, T. Bessho, and M. Sato, Phys. Rev. Lett. **123**, 066405 (2019).
[48] J. C. Budich, J. Carlström, F. K. Kunst, and E. J. Bergholtz, Phys. Rev. B **99**, 041406(R) (2019).
[49] M. Stålhammar and E. J. Bergholtz, Phys. Rev. B **104**, L201104 (2021).
[50] P. Delplace, T. Yoshida, and Y. Hatsugai, Phys. Rev. Lett. **127**, 186602 (2021).
[51] D. Bernard and A. LeClair, in *Statistical Field Theories*, NATO Science Series, edited by A. Cappelli and G. Mussardo (Springer Netherlands, Dordrecht, 2002), pp. 207–214.
[52] K. Kawabata, K. Shiozaki, M. Ueda, and M. Sato, Phys. Rev. X **9**, 041015 (2019).
[53] S. Lieu, Phys. Rev. B **98**, 115135 (2018).
[54] H. Zhou and J. Y. Lee, Phys. Rev. B **99**, 235112 (2019).
[55] E. J. Bergholtz, J. C. Budich, and F. K. Kunst, Rev. Mod. Phys. **93**, 015005 (2021).
[56] L. Li, C. H. Lee, and J. Gong, Phys. Rev. B **100**, 075403 (2019).
[57] H. B. Nielsen and M. Ninomiya, Phys. Lett. **105B**, 219 (1981).
[58] H. B. Nielsen and M. Ninomiya, Nucl. Phys. **B185**, 20 (1981).
[59] H. B. Nielsen and M. Ninomiya, Nucl. Phys. **B193**, 173 (1981).
[60] Z. Yang, A. P. Schnyder, J. Hu, and C.-K. Chiu, Phys. Rev. Lett. **126**, 086401 (2021).
[61] J. Y. Lee, J. Ahn, H. Zhou, and A. Vishwanath, Phys. Rev. Lett. **123**, 206404 (2019).
[62] R. Yu, X. L. Qi, A. Bernevig, Z. Fang, and X. Dai, Phys. Rev. B **84**, 075119 (2011).
[63] A. Alexandradinata, X. Dai, and B. A. Bernevig, Phys. Rev. B **89**, 155114 (2014).
[64] Z. Zhu, G. W. Winkler, Q. S. Wu, J. Li, and A. A. Soluyanov, Phys. Rev. X **6**, 031003 (2016).
[65] W. A. Benalcazar, B. A. Bernevig, and T. L. Hughes, Science **357**, 61 (2017).
[66] X.-W. Luo and C. Zhang, Phys. Rev. Lett. **123**, 073601 (2019).
[67] H. Hu and E. Zhao, Phys. Rev. Lett. **126**, 010401 (2021).
[68] See Supplemental Material at http://link.aps.org/supplemental/10.1103/PhysRevLett.128.226401 for details, which includes Refs. [17,64,69–75].
[69] Z. Ren, D. Liu, E. Zhao, C. He, K. K. Pak, J. Li, and G.-B. Jo, Nat. Phys. **18**, 385 (2022).
[70] X. Feng, W. Wu, Y. Huang, Z.-M. Yu, and S. A. Yang, Phys. Rev. B **104**, 115116 (2021).

[71] T.-T. Zhang, Z.-M. Yu, W. Guo, D. Shi, G. Zhang, and Y. Yao, J. Phys. Chem. Lett. **8**, 5792 (2017).
[72] D.-W. Zhang, S.-L. Zhu, and Z. D. Wang, Phys. Rev. A **92**, 013632 (2015).
[73] Z. Wu, L. Zhang, W. Sun, X.-T. Xu, B.-Z. Wang, S.-C. Ji, Y. Deng, S. Chen, X.-J. Liu, and J.-W. Pan, Science **354**, 83 (2016).
[74] Z.-Y. Wang, X.-C. Cheng, B.-Z. Wang, J.-Y. Zhang, Y.-H. Lu, C.-R. Yi, S. Niu, Y. Deng, X.-J. Liu, S. Chen, and J.-W. Pan, Science **372**, 271 (2021).
[75] M. Ben Dahan, E. Peik, J. Reichel, Y. Castin, and C. Salomon, Phys. Rev. Lett. **76**, 4508 (1996).
[76] Y. Ashida, Z. Gong, and M. Ueda, Adv. Phys. **69**, 249 (2020).
[77] C. Fang, M. J. Gilbert, X. Dai, and B. A. Bernevig, Phys. Rev. Lett. **108**, 266802 (2012).
[78] L. Fu, C. L. Kane, and E. J. Mele, Phys. Rev. Lett. **98**, 106803 (2007).
[79] X.-L. Qi, T. L. Hughes, and S.-C. Zhang, Phys. Rev. B **78**, 195424 (2008).
[80] S. Ryu, J. E. Moore, and A. W. W. Ludwig, Phys. Rev. B **85**, 045104 (2012).
[81] M. M. Denner, A. Skurativska, F. Schindler, M. H. Fischer, R. Thomale, T. Bzdušek, and T. Neupert, Nat. Commun. **12**, 5681 (2021).
[82] Y. Xu, Front. Phys. **14**, 43402 (2019).
[83] D.-W. Zhang, Y.-Q. Zhu, Y. X. Zhao, H. Yan, and S.-L. Zhu, Adv. Phys. **67**, 253 (2018).
[84] T. Köhler, K. Góral, and P. S. Julienne, Rev. Mod. Phys. **78**, 1311 (2006).
[85] C. Chin, R. Grimm, P. Julienne, and E. Tiesinga, Rev. Mod. Phys. **82**, 1225 (2010).
[86] W. H. Zurek, U. Dorner, and P. Zoller, Phys. Rev. Lett. **95**, 105701 (2005).
[87] S. Hofferberth, I. Lesanovsky, B. Fischer, T. Schumm, and J. Schmiedmayer, Nature (London) **449**, 324 (2007).
[88] A. Polkovnikov, K. Sengupta, A. Silva, and M. Vengalattore, Rev. Mod. Phys. **83**, 863 (2011).